# Acoustic Carpets

Maciej Janowicz, Joanna Kaleta, Piotr Wrzeciono, Andrzej Zembrzuski
*Faculty of Applications of Informatics and Mathematics – WZIM*
*Warsaw University of Life Sciences – SGGW*
*Nowoursynowska 159, 02-775 Warsaw, Poland*
`http://www.wzim.sggw.pl`

**Abstract.** Initial-boundary value problem for linear acoustics has been solved in two spatial dimensions. It has been assumed that the initial acoustic field consists of two Gaussian distributions. Dirichlet boundary conditions with zero acoustic pressure at the boundaries have been imposed. The solution has been obtained with the help of a split-operator technique which resulted in a cellular automaton with uncountably many internal states. To visualize the results, the Python library `matplotlib` has been employed. It has been shown that attractive graphical output results in both the transient and stationary regimes. The visualization effects are similar to, but different from, the well-known quantum-mechanical carpets.

**Key words:** acoustics, Euler equations, split-operator method, visualization of physical fields.

## 1. Introduction

As is well known, interference effects omnipresent in the propagation of both linear and non-linear physical fields, very often lead to formation of beautiful patterns. Let us only mention here caustic patterns which can be in coffee cup due to the multiple reflection of light rays with the cup serving as a kind of quasi-cylindrical mirror. Many interesting and important physical effects are known in quantum mechanics due to the interference of probability waves. This includes formation of sometimes spectacular patterns emerging in the propagation of probability waves in an infinite potential well [2, 3, 4, 5]. Very interesting and beautiful images have been obtained by simulation of the dynamics of quantum mechanical wavepackets provided that generic initial conditions have been assumed. By *generic* initial conditions we mean those with many modes being initially excited. Interesting revivals of patterns have been reported.

Needless to say, one can and should expect appearance of similarly interesting structures in other physical fields, for instance, electromagnetic or acoustic. The role of quantum-mechanical infinite-well potential is naturally played by perfectly reflecting walls. It is to be mentioned that such walls actually do not exist. Nevertheless, a model with perfectly reflecting walls is a convenient starting point and can provide a reasonable approximation if we do not consider the fields too close to such mirrors.

In this work we concentrate on the case of evolution of acoustic fields in two spatial dimensions. The main body of the paper is organized as follows. In Section 2 we provide

Euler's partial differential equations which constitute the mathematical model of our system. In Section 3 a simple but efficient algorithm to integrate those equations is worked out. Section 4 contains a series of figures in which our results are illustrated. Some concluding remarks can be found in Section 5.

## 2. The model

We are about to solve the following system of the partial differential equations [1]:

$$\frac{\partial p}{\partial \tau} + \frac{\partial v_x}{\partial \xi} + \frac{\partial v_y}{\partial \eta} = 0\,, \tag{1}$$

$$\frac{\partial v_x}{\partial \tau} + \frac{\partial p}{\partial \xi} = 0\,, \tag{2}$$

$$\frac{\partial v_y}{\partial \tau} + \frac{\partial p}{\partial \eta} = 0\,. \tag{3}$$

All quantities in the above system, including the independent variables, have been made dimensionless. The quantity $p$ has the physical meaning of the acoustic pressure while $v_x$ and $v_y$ are two components of the field of velocity of particles. The variable $\tau$ is the dimensionless time while $\xi$ and $\eta$ are dimensionless coordinates in the plane.

The above system describes propagation of the acoustic field in two spatial dimensions. In this work we will employ the simple Dirichlet boundary conditions: $p = 0$ on any boundary.

Equations (1)-(3) can be represented in a matrix form:

$$\frac{\partial}{\partial \tau}\begin{pmatrix} p \\ v_x \\ v_y \end{pmatrix} = \widehat{\mathbf{M}}\begin{pmatrix} p \\ v_x \\ v_y \end{pmatrix}, \tag{4}$$

where the matrix operator $\widehat{\mathbf{M}}$ is equal to

$$-\begin{pmatrix} 0 & \frac{\partial}{\partial \xi} & \frac{\partial}{\partial \eta} \\ \frac{\partial}{\partial \xi} & 0 & 0 \\ \frac{\partial}{\partial \eta} & 0 & 0 \end{pmatrix}. \tag{5}$$

In the following section this matrix notation will be used to develop a split-operator algorithm for numerical computations of $(p, v_x, v_y)$.

## 3. Split-operator algorithm

Equations (1)-(3) can be formally integrated to give:

$$\begin{pmatrix} p(\tau+\Delta\tau,\xi,\eta) \\ v_x(\tau+\Delta\tau,\xi,\eta) \\ v_y(\tau+\Delta\tau,\xi,\eta) \end{pmatrix} = \exp(\widehat{\mathbf{M}}\Delta\tau) \begin{pmatrix} p(\tau,\xi,\eta) \\ v_x(\tau,\xi,\eta) \\ v_y(\tau,\xi,\eta) \end{pmatrix} . \tag{6}$$

Let us write the matrix $\widehat{\mathbf{M}}$ as a sum of four terms:

$$\widehat{\mathbf{M}} = \widehat{\mathbf{M}}_1 + \widehat{\mathbf{M}}_2 + \widehat{\mathbf{M}}_3 + \widehat{\mathbf{M}}_4 \,, \tag{7}$$

where

$$\widehat{\mathbf{M}}_1 = \widehat{\mathbf{M}}_3 = -\frac{1}{2} \begin{pmatrix} 0 & \frac{\partial}{\partial\xi} & 0 \\ \frac{\partial}{\partial\xi} & 0 & 0 \\ 0 & 0 & 0 \end{pmatrix} , \tag{8}$$

$$\widehat{\mathbf{M}}_2 = \widehat{\mathbf{M}}_4 = -\frac{1}{2} \begin{pmatrix} 0 & 0 & \frac{\partial}{\partial\eta} \\ 0 & 0 & 0 \\ \frac{\partial}{\partial\eta} & 0 & 0 \end{pmatrix} . \tag{9}$$

Let us notice here that the matrices with even and odd indices do not commute.

For small $\Delta\tau$ we can approximately "split" the matrix exponential $\exp(\widehat{\mathbf{M}}\Delta\tau)$ as follows [6, 7, 8]

$$\exp(\widehat{\mathbf{M}}\Delta\tau) \approx \prod_{n=1}^{4} \exp(\widehat{\mathbf{M}}_n\Delta\tau) \,. \tag{10}$$

The following remark is necessary here. In our numerical simulations $\Delta\tau$ is actually not small: it is exactly equal to 2. However, it is sufficient to require that $\Delta\tau$ be small when compared to characteristic lengths introduced by the initial conditions (or boundary conditions, or, in a more general settings, by frequencies of the external currents). In our case $\Delta\tau$ will be significantly smaller that the half-widths of Gaussians which form the initial conditions.

Taking into account that

$$\begin{aligned}
\exp(\widehat{\mathbf{M}}_1\Delta\tau) &= \begin{pmatrix}1&0&0\\0&1&0\\0&0&0\end{pmatrix}\cosh\left(\frac{\Delta\tau}{2}\frac{\partial}{\partial\xi}\right)+\\
&-\begin{pmatrix}0&1&0\\1&0&0\\0&0&0\end{pmatrix}\sinh\left(\frac{\Delta\tau}{2}\frac{\partial}{\partial\xi}\right)+\begin{pmatrix}0&0&0\\0&0&0\\0&0&1\end{pmatrix}, \qquad (11)\\
\exp(\widehat{\mathbf{M}}_2\Delta\tau) &= \begin{pmatrix}1&0&0\\0&0&0\\0&0&1\end{pmatrix}\cosh\left(\frac{\Delta\tau}{2}\frac{\partial}{\partial\eta}\right)+\\
&-\begin{pmatrix}0&0&1\\0&0&0\\1&0&0\end{pmatrix}\sinh\left(\frac{\Delta\tau}{2}\frac{\partial}{\partial\eta}\right)+\begin{pmatrix}0&0&0\\0&1&0\\0&0&0\end{pmatrix}, \qquad (12)
\end{aligned}$$

as well as considering the simple action of hyperbolic sine and cosine functions of first-order operators on any function $f(\xi,\eta)$, e.g.:

$$\begin{aligned}
\cosh\left(\frac{\Delta\tau}{2}\frac{\partial}{\partial\eta}\right)f(\xi,\eta) &= \frac{1}{2}\left[f(\xi,\eta+\frac{\Delta\tau}{2})+f(\xi,\eta-\frac{\Delta\tau}{2})\right], \qquad (13)\\
-\sinh\left(\frac{\Delta\tau}{2}\frac{\partial}{\partial\eta}\right)f(\xi,\eta) &= \frac{1}{2}\left[f(\xi,\eta-\frac{\Delta\tau}{2})-f(\xi,\eta+\frac{\Delta\tau}{2})\right], \qquad (14)
\end{aligned}$$

we end up with a simple four-step algorithm to integrate (1)-(3). For instance, the first step is obtained upon using the exponential of $\widehat{\mathbf{M}}_4$:

$$\begin{aligned}
p^{(1)}(\xi,\eta) &= \frac{1}{2}\left[p(\tau,\xi,\eta+\frac{\Delta\tau}{2})+p(\tau,\xi,\eta-\frac{\Delta\tau}{2})\right]+\\
&-\frac{1}{2}\left[v_y(\tau,\xi,\eta+\frac{\Delta\tau}{2})-v_y(\tau,\xi,\eta-\frac{\Delta\tau}{2})\right], \qquad (15)\\
v_x^{(1)}(\xi,\eta) &= v_x(\tau,\xi,\eta), \qquad (16)\\
v_y^{(1)}(\xi,\eta) &= -\frac{1}{2}\left[p(\tau,\xi,\eta+\frac{\Delta\tau}{2})-p(\tau,\xi,\eta-\frac{\Delta\tau}{2})\right]+\\
&\frac{1}{2}\left[v_y(\tau,\xi,\eta+\frac{\Delta\tau}{2})+v_y(\tau,\xi,\eta-\frac{\Delta\tau}{2})\right]. \qquad (17)
\end{aligned}$$

In the second step, using exponential of $\widehat{\mathbf{M}}_3$ we obtain:

$$\begin{aligned} p^{(2)}(\xi,\eta) &= \frac{1}{2}\left[p^{(1)}(\xi+\frac{\Delta\tau}{2},\eta)+p^{(1)}(\xi-\frac{\Delta\tau}{2},\eta)\right]+ \\ &\quad -\frac{1}{2}\left[v_x^{(1)}(\xi+\frac{\Delta\tau}{2},\eta)-v_x^{(1)}(\xi-\frac{\Delta\tau}{2},\eta)\right], \qquad (18) \\ v_x^{(2)}(\xi,\eta) &= -\frac{1}{2}\left[p^{(1)}(\xi+\frac{\Delta\tau}{2},\eta)-p^{(1)}(\xi-\frac{\Delta\tau}{2},\eta)\right]+ \\ &\quad \frac{1}{2}\left[v_x^{(1)}(\xi+\frac{\Delta\tau}{2},\eta)+v_x^{(1)}(\xi-\frac{\Delta\tau}{2},\eta)\right], \qquad (19) \\ v_y^{(2)}(\xi,\eta) &= v_y^{(1)}(\xi,\eta), \qquad (20) \end{aligned}$$

and so on.

We have discretized our simulation cell, being a square, as $\xi = m\Delta\xi$, $\eta = n\Delta\eta$, $m,n = 0,1,...,N-1$, and set $\Delta\xi = \Delta\eta = 1$, $\Delta\tau = 2$. Thus, the fields $p, v_x, v_y$ have become functions of discrete variables $m$ and $n$. The boundary conditions $p = 0$ result in the following prescription for $v_x(0,n)$, $v_x(N-1,n)$, $v_y(m,0)$, $v_y(m,N-1)$:

$$\begin{aligned} v_x(0,n) &= -p(1,n)+v_x(1,n), \\ v_x(N-1,n) &= p(N-2,n)+v_x(N-2,n), \\ v_y(m,0) &= -p(m,1)+v_y(m,1), \\ v_y(m,N-1) &= p(m,N-2)+v_y(m,N-2). \end{aligned}$$

Let us notice that the algorithm per se is unitary and it preserves the energy exactly. However, the numerical boundary conditions slightly spoil the energy conservation so that it exhibits oscillations with amplitudes up to 0.5%.

The above algorithm while being simply a particular version of finite-difference method, also forms a kind of cellular automaton with uncountably many states. Similar automata have also been constructed e.g. in [9, 10, 11].

## 4. Numerical results

In all our numerical simulations the size $N$ of the computational cell has been equal to 1000. The initial conditions have been of the form:

$$p(m,n) = 10\sum_{i=0}^{1}\exp(-((m-m_i)^2+(n-n_i)^2)/(2\sigma^2))/(2\pi\sigma^2)$$

with $m_0 = n_0 = N/4$, $m_1 = n_1 = 3N/4$. The initial velocity has been assumed to vanish everywhere. We have performed simulations for several values of $\sigma$.

The the dependence of $|p|$ on $(\xi, \eta)$ for various $\tau$ and for $\sigma = 20$ has been shown in Figure 1, and further on, in Figure 2 for $\sigma = 60$.

In addition, we have also performed simulations with vanishing initial conditions but with point-like external current in the form of an additional boundary condition

$$p(m_0, n_0) = p_0 \sin(\nu\tau),$$

with $p_0 = 1$ and $\nu = 0.01$ (thus, $\Delta\tau \ll 1/\nu$). The results are shown in Figure 3.

Let us ask an important question whether we can draw any conclusions from the images in Figures 1-3. The answer is, naturally, affirmative. Just by looking at these images we may infer that any "geometrooptical", i.e. ray-tracing approach to the system must immediately result in a failure. The interference effects kill the well-defined wave packets and the "carpet" structure arises. On the other hand, the initial presence of small-width wavepackets leads to a fine, granular structure of the carpet. Larger widths provide larger and better visible structures in the square.

## 5. Conclusion

In this paper we have provided a simple yet efficient cellular-automaton-like, unitary algorithm to integrate Euler's equations of linear acoustics. Numerical simulations of the dynamics of acoustic fields starting with two Gaussian wavepackets have been carried out inside a square with perfectly reflecting walls. What is more, similar simulations have been performed for the fields with zeroth initial condition but under the presence of an external source with sinusoidal time variation. Our results have been illustrated with the help of the Python library `matplotlib`. We believe they form a valuable supplement to what is known about interference in linear field structures evolving inside very high-quality resonators.

Let us notice that visualization has, of course, already become a standard tool of acoustic analysis. Let us quote only recent papers [12, 13, 14] in this connection.

We plan to investigate further similar systems with special emphasis on the presence of vortices and other topological structures in the field.

## References

[1] Morse P. *Vibrations and Sound*. McGraw-Hill, New York, 1948.

[2] Marzoli I., Saif F., Białynicki-Birula I., Friesch, O.M., Kaplan, A.E., and Schleich W.P. Quantum carpets made simple. *Acta Phys.Slov.* **48**:323-333, 1998

[3] Hall M.J.W., Reineker M.S. and Schleich W.P. Unravelling quantum carpets: a travelling wave approach. *J. Phys. A* **32**:8275-8291, 1999.

[4] Kaplan A.E., Marzoli I., Lamb Jr., W.E., and Schleich W.P. Multimode interference: Highly regular pattern formation in quantum wave-packet evolution. *Phys. Rev. A* **61**:032101, 2000.

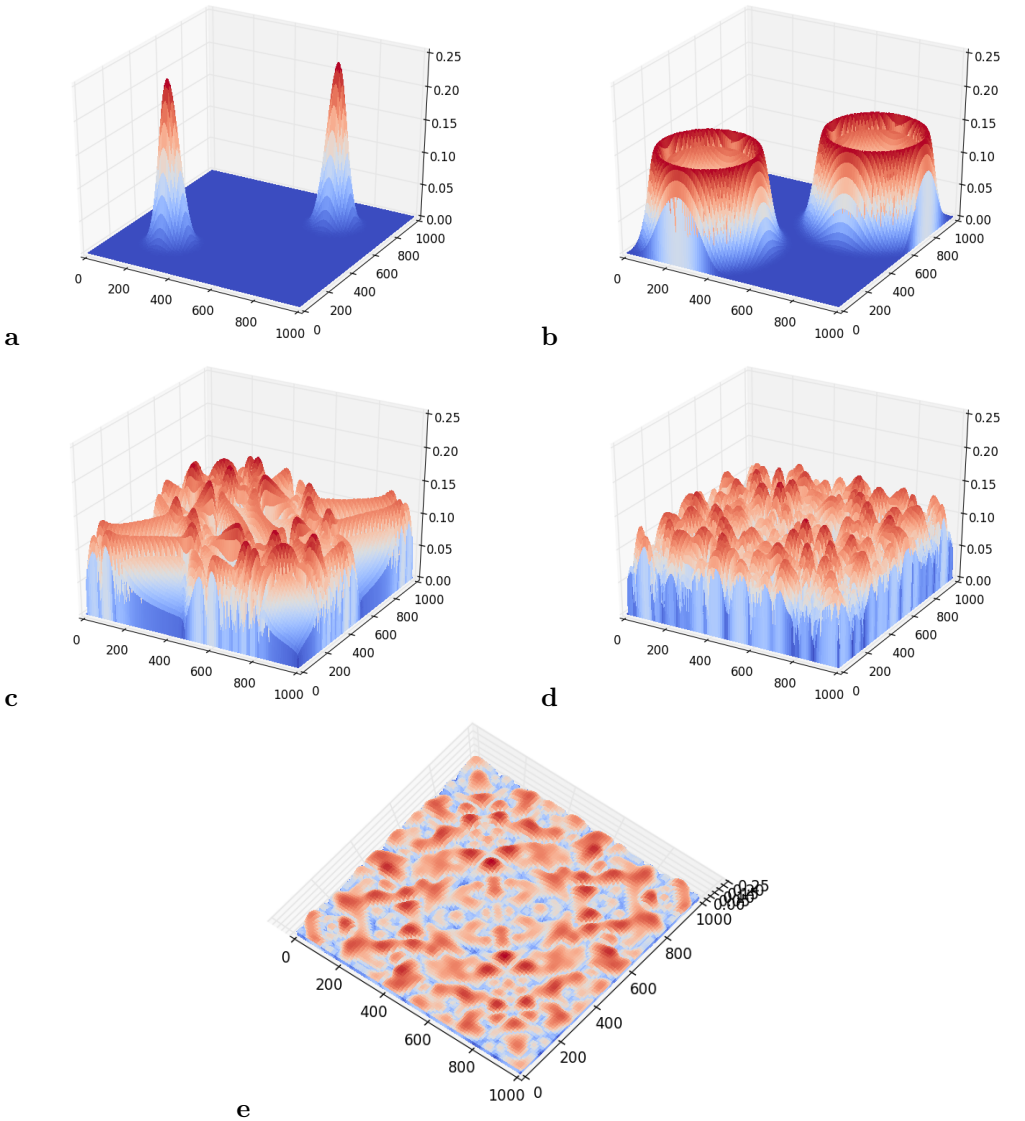


Fig. 1. Snapshots of the time evolution of acoustic field from two Gaussian wavepackets for $\sigma = 20.0$ (see text). The quantity $|p|^{1/4}$ is plotted as a function of $\xi$ and $\eta$ for several $\tau$. (**a**) $\tau = 1$; (**b**) $\tau = 100$; (**c**) $\tau = 500$; (**d**) $\tau = 5000$; (**e**) same as d but at a different projection.

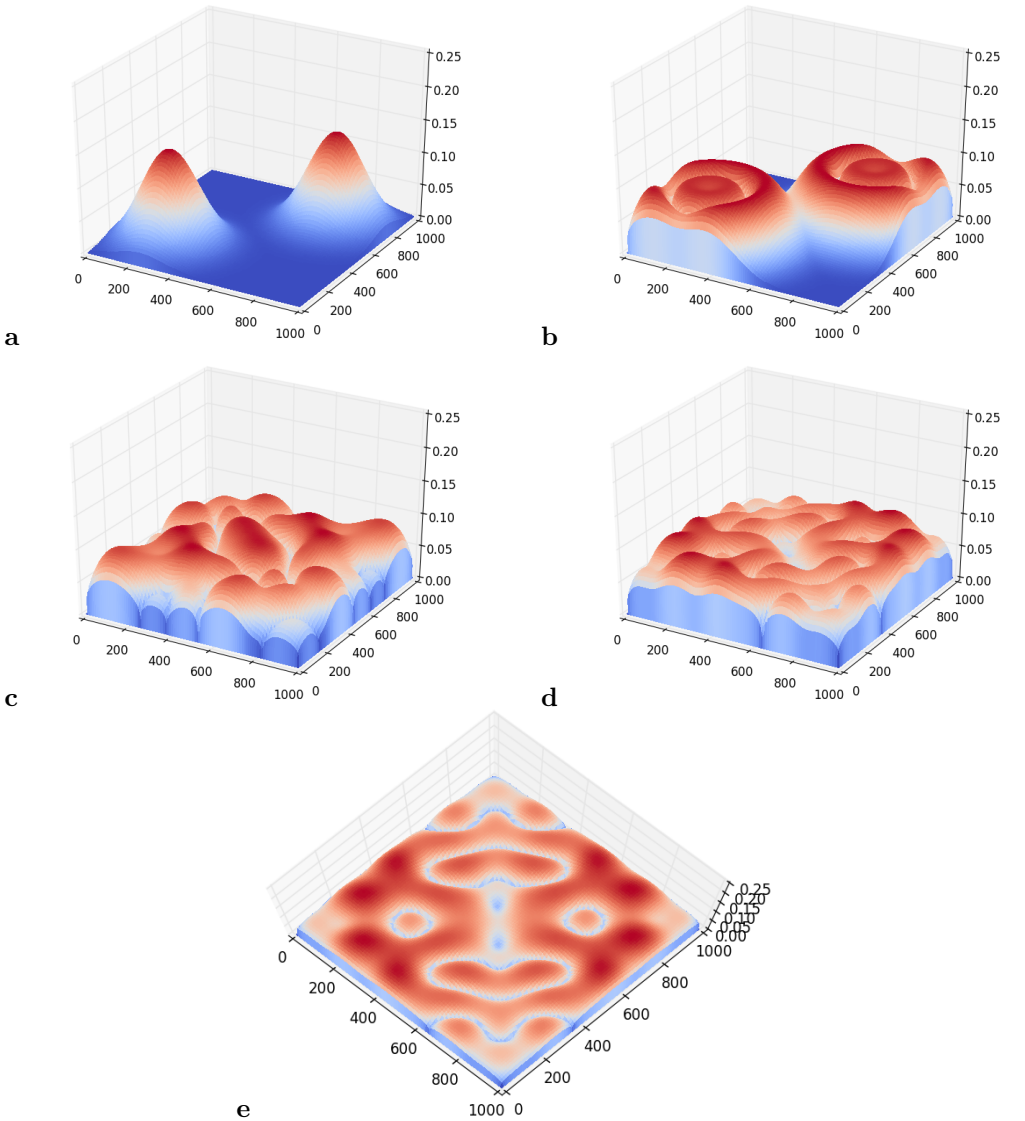


Fig. 2. Snapshots of the time evolution of acoustic field from two Gaussian wavepackets for $\sigma = 60.0$ (see text). The quantity $|p|^{1/4}$ is plotted as a function of $\xi$ and $\eta$ for several $\tau$: (**a**) $\tau = 1$, (**b**) $\tau = 100$, (**c**) $\tau = 500$, (**d**) $\tau = 5000$. (**e**) Same as **d** but at a different projection.

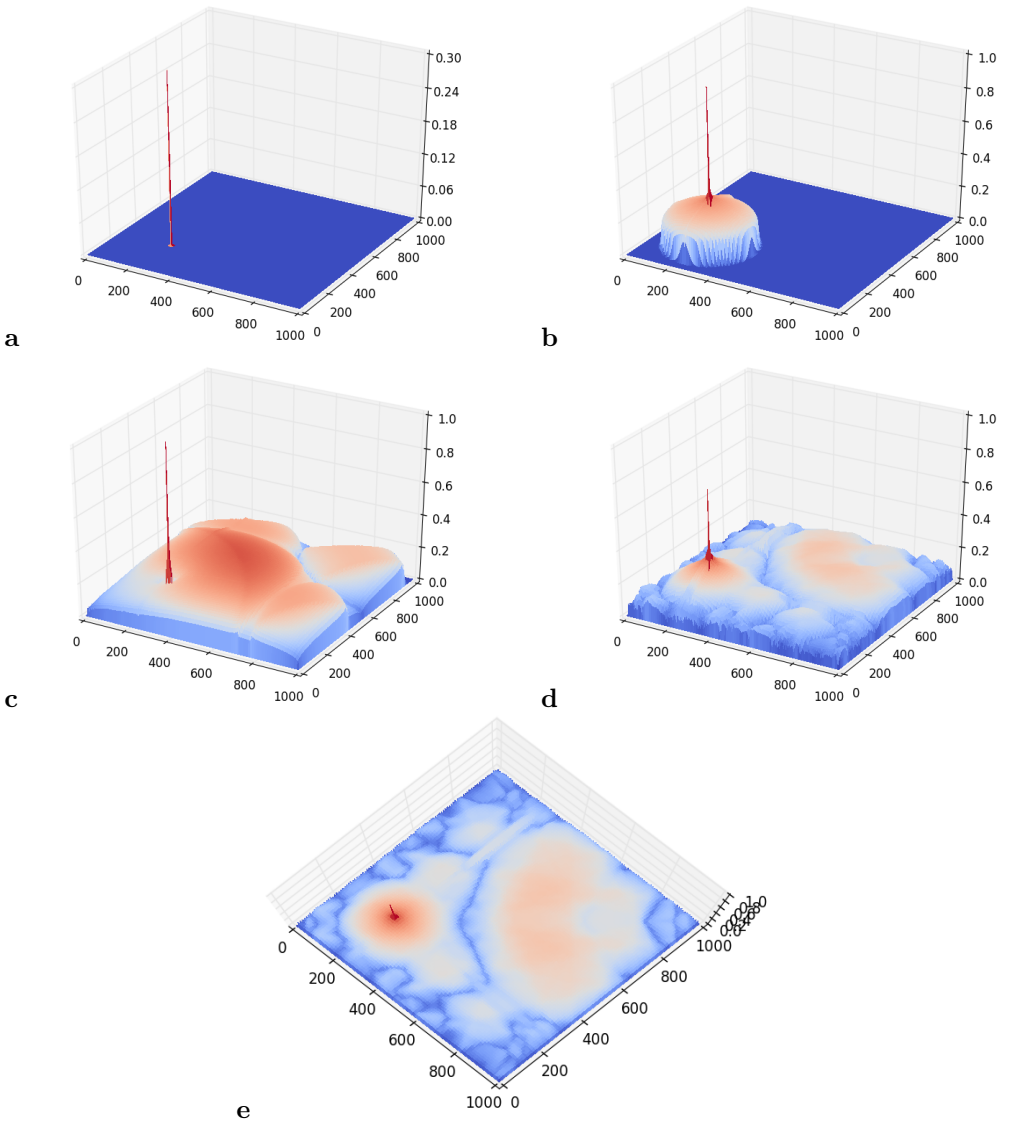


Fig. 3. Snapshots of the time evolution of acoustic field with zeroth initial conditions but in the presence of external current (see text). The quantity $|p|^{1/4}$ is plotted as a function of $\xi$ and $\eta$ for several $\tau$: (**a**) $\tau = 1$, (**b**) $\tau = 100$, (**c**) $\tau = 500$, (**d**) $\tau = 5000$. (**e**) Same as **d** but at a different projection.

[5] Belloni M., Doncheski M.A., and Robinett R.W. Wigner quasi-probability distribution for the infinite square well: Energy eigenstates and time-dependent wave packets. *Am. J. Phys.* **72**:1183-1192, 2004.

[6] Trotter H.F. On the product of semi-groups of operators. *Proc. Am. Math. Soc.* **10**:545-551, 1959.

[7] Feit M.D., Fleck Jr. J.A., and Steiger A. Solution of the Schrödinger equation by a spectral method. *J. Comp. Phys.* **47**:412-433, 1982.

[8] Suzuki M. Decomposition formulas of exponential operators and Lie exponentials with some applications to quantum mechanics and statistical physics. *J. Math. Phys.* **26**:601-612, 1985.

[9] Białynicki-Birula I. Weyl, Dirac, and Maxwell equations on a lattice as unitary cellular automata. *Phys. Rev. D* **49**:6920, 1994.

[10] Succi S. *The Lattice Boltzmann Equation: For Fluid Dynamics and Beyond*. Clarendon Press, Oxford, 2001.

[11] Janowicz, M.W., Ashbourn J.M.A., Orłowski A. and Mostowski J. Cellular automaton approach to electromagnetic wave propagation in dispersive media. *Proc. Roy. Soc. London Ser. A* **462**:2927-2948, 2006.

[12] Miyasaka C., Telschow K.L., Tittmann B.R., Sadler J.T., and Park I.K. Direct visualisation of acoustic waves propagation within a single anisotropic crystalline plate with hybrid acoustic imaging system. *Research in Nondesctructive Evaluation* **23**:197-206, 2012.

[13] Szczodrak M., Kurowski A., Kotus J., Czyżewski A., and Kostek B. A system for acoustic field measurement employing Cartesian robot. *Metrol. Meas. Syst.* **23**:333-343, 2016.

[14] Rambach R.W., Taiber J., Scheck C.M.L., Meyer C., Reboud J., Cooper J.M., and Franke T. Visualization of Surface Acoustic Waves in Thin Liquid Films. *Sci. Rep.* **6**:21980, 2016. DOI:10.1038/srep21980.